

1       **Making Archean cratonic roots by lateral compression: a two-**  
2       **stage thickening and stabilization model**

3

4       **Abstract**

5       Archaean tectonics was capable of producing virtually indestructible cratonic mantle lithosphere,  
6       but the dominant mechanism of this process remains a topic of considerable discussion. Recent  
7       geophysical and petrological studies have refuelled the debate by suggesting that thickening and  
8       associated vertical movement of the cratonic mantle lithosphere after its formation are essential  
9       ingredients of the cratonization process. Here we present a geodynamical study that focuses on  
10      how the thick stable cratonic lithospheric roots can be made in a thermally evolving mantle.  
11      Our numerical experiments explore the viability of a cratonization process in which depleted  
12      mantle lithosphere grows via lateral compression into a >200-km thick, stable cratonic root and  
13      on what timescales this may happen. Successful scenarios for craton formation, within the  
14      bounds of our models, are found to be composed of two stages: an initial phase of tectonic  
15      shortening and a later phase of gravitational self-thickening. The initial tectonic shortening of  
16      previously depleted mantle material is essential to initiate the cratonization process, while the  
17      subsequent gravitational self-thickening contributes to a second thickening phase that is compa-  
18      rable in magnitude to the initial tectonic phase. Our results show that a combination of intrinsic  
19      compositional buoyancy of the cratonic root, rapid cooling of the root after shortening, and the  
20      long-term secular cooling of the mantle prevents a Rayleigh-Taylor type collapse, and will sta-  
21      bilize the thick cratonic root for future preservation. This two- stage thickening model provides  
22      a geodynamically viable cratonization scenario that is consistent with petrological and geophys-  
23      ical constraints.

24

25

26

27

28

29

30

31

## 33 **1 Introduction**

34 Cratons, the oldest parts of the Earth's lithosphere, owe their longevity and stability to their  
35 chemically distinct, highly melt-depleted cratonic roots [Jordan, 1975; Carlson *et al.*, 2005;  
36 Burov, 2011; Pearson and Wittig, 2014; Wang *et al.*, 2014]. The formation of these roots, how-  
37 ever, continues to be debated, and three main endmember hypotheses for the formation of cra-  
38 tonic lithosphere have been proposed [e.g., Pearson and Wittig, 2008; Arndt *et al.*, 2009; Lee *et*  
39 *al.*, 2011]. First, a thick, stable mantle lithosphere forms through melting in a large mantle  
40 plume head. A second way to form cratons can be the accretion and stacking of segments of  
41 oceanic lithosphere. Finally, accretion and thickening of already buoyant arc lithosphere might  
42 be capable of producing stable keels. In particular, there has been much debate regarding the  
43 relative importance of plume-related melting and vertical accretion versus lateral accretion and  
44 thickening by tectonic processes [Griffin *et al.*, 2003; Lee, 2006; Aulbach, 2012; Pearson and  
45 Wittig, 2014]. The dynamics associated with compressional thickening has long been proposed  
46 as an important aspect of cratonization [Jordan, 1978]. Recent studies suggest that vertical tec-  
47 tonics might have played a more important role in the Archean than it does today [Bélarard *et al.*,  
48 2003; Sleep, 2005; Sizova *et al.*, 2015]. While compressional models of cratonic lithosphere  
49 have been long proposed and recently popularised [e.g. McKenzie and Priestley, 2016] there  
50 remains, as yet, no in-depth geodynamic model that studies the viability of this process and the  
51 timescale over which it may operate, within the framework of modern geodynamical modelling.

52 The melting depth of the peridotitic protolith is one of the key constraints for the craton  
53 formation process [Herzberg, 1999; Canil, 2004; Pearson and Wittig, 2008, 2014; Aulbach,  
54 2012; Lee and Chin, 2014]. High pressure (3-6 GPa) melting conditions of craton protoliths ob-  
55 tained from bulk-rock major element studies have been used as evidence for a plume origin [e.g.  
56 Pearson *et al.*, 1995; Herzberg, 1999; Aulbach, 2012]. However, this approach is vulnerable to  
57 the effects that later metasomatic processes have on modifying the bulk compositions used to  
58 constrain melting depth [Lee, 2006; Pearson and Wittig, 2008]. In contrast, results from mildly  
59 incompatible trace elements that are more robust to metasomatic processes argue for a low pres-  
60 sure origin of cratonic peridotite (<3 GPa) [Canil, 2004; Wittig *et al.*, 2008]. Lee and Chin  
61 [2014] explicitly calculated the temperature and pressure conditions of peridotite melting events  
62 through bulk FeO and MgO measurements of the residual peridotite. They concluded that Ar-  
63 chean cratonic peridotites were likely formed at melting temperatures of 1400-1750°C and pres-  
64 sures of 1-5 GPa (30-150 km), and subsequently transported to depths of 3-7.5 GPa (90-200  
65 km), where they cooled and stabilized.

66 *Cooper and Miller* [2014] studied the thickening of buoyant residual mantle material over  
67 a mantle down-welling using geodynamical modelling and suggest that the observed seismic  
68 'mid-lithospheric discontinuities' might be explained by localized deformation during the thick-  
69 ening phase of the cratonic lithosphere. The driving force for this vertical movement of depleted

70 peridotite is either an external tectonic force or internal gravitational forces. Studies of the secu-  
 71 lar thermal evolution of the cratonic lithosphere demonstrate that the often proposed isopycnic  
 72 state of cratonic lithosphere is an inherently ephemeral phenomenon due to the evolution of  
 73 negative thermal buoyancy [Eaton and Perry, 2013]. Laboratory experiments on the physical  
 74 properties of depleted mantle rocks indicate that subcratonic mantle formed shallower than ~110  
 75 km is negatively buoyant with respect to adiabatic mantle [Schutt and Lesher, 2006], which  
 76 suggests that such residues are capable of gravitationally-driven vertical movement.

77 Both petrological evidence and geophysical constraints indicate that vertical movement of  
 78 lithosphere is likely during craton formation. This suggests that shortening and thickening of  
 79 depleted mantle material may be common, and might provide a viable geodynamical scenario  
 80 for the cratonization process. However, the controlling factors that enable both initial thickening  
 81 and subsequent, long-term stabilization of cratonic lithosphere remain unclear and have yet to  
 82 be fully explored. In particular how the cratons evolve to their stable roots from an unstable  
 83 thickening phase, without under-going Rayleigh-Taylor collapse [e.g. Houseman and Molnar,  
 84 1997] requires more investigation. Therefore, in this study, we present a set of numerical exper-  
 85 iments that investigate how cratons might have grown to their current thicknesses, via lateral  
 86 compression, within a thermally evolving mantle, while preserving long-term stability. We ex-  
 87 plore the potentially important model parameters related to craton thickening and stabilization.

## 88 **2 Model description**

### 89 **2.1 Governing equations**

90 We use a Cartesian version of the finite element code Citcom [Moresi and Solomatov, 1995;  
 91 Zhong et al., 2000; van Hunen et al., 2005] to solve the incompressible flow with Boussinesq  
 92 approximations. The non-dimensional governing equations for mass, momentum, energy con-  
 93 servation are:

$$94 \quad \nabla \cdot \mathbf{u} = 0, \quad (1)$$

$$95 \quad -\nabla P + \nabla \cdot (\eta(\nabla \mathbf{u} + \nabla \mathbf{u}^T)) + (RaT - Rb_i C_i) \mathbf{e}_z = 0, \quad (2)$$

$$96 \quad \frac{\partial T}{\partial t} + \mathbf{u} \cdot \nabla T = \nabla^2 T + Q_0. \quad (3)$$

97 A standard non-dimensionalisation is used with  
 98  $x = x' h, t = t' h^2 / \kappa, \eta = \eta' \eta_0, T = (T' + T_0) \Delta T$ , where the primes of the non-dimensional pa-  
 99 rameters are dropped for clarity in the above equations. The dimensional physical parameters  
 100 are listed and explained in Table 1. The thermal and compositional Rayleigh number  $Ra$  and  $Rb_i$   
 101 are defined as:

102

103 
$$Ra = \frac{\alpha \rho_0 g \Delta T h^3}{\kappa \eta_0}, \quad (4)$$

104 
$$Rb_i = \frac{\delta \rho_i g h^3}{\kappa \eta_0}. \quad (5)$$

105 We use a composite rheology of dislocation and diffusion creep which assumes that the  
 106 melt-depleted mantle is dry and therefore more viscous than the undepleted mantle [Hirth *et al.*,  
 107 2000; Karato, 2010]. The rheology setup is similar to Wang *et al.* [2015b], but we ignore the  
 108 pressure dependence of the rheology in order to reduce the model complexity and focus on litho-  
 109 sphere dynamics. The composition-dependent viscosities for dislocation creep and diffusion  
 110 creep are defined as:

111 
$$\eta_{dl} = A \left( \frac{1}{n} \right) \dot{\epsilon}^{\left( \frac{1-n}{n} \right)} \exp \left( \frac{E}{nRT} \right) \times \Delta \eta, \quad (7)$$

112 
$$\eta_{df} = B \exp \left( \frac{E}{RT} \right) \times \Delta \eta^n \quad (8)$$

113 In which  $\Delta \eta$  is the strengthening that results from melt depletion. In addition, we apply a yield-  
 114 ing mechanism [van Hunen and Allen, 2011] to consider the brittle yielding of strong litho-  
 115 sphere during the imposed shortening process:

116 
$$\eta_y = \frac{\min(\tau_0 + \mu P, \tau_{max})}{\dot{\epsilon}}, \quad (9)$$

117 with the description of the rheological parameters listed in Table 1. Therefore, the effective  
 118 viscosity is defined as:

119 
$$\eta_{eff} = \min(\eta_{dl}, \eta_{df}, \eta_y). \quad (10)$$

120 In contrast to the mantle, the crust is assigned a weaker rheology in order to take into ac-  
 121 count the potentially important effects of relatively weak and buoyant crust. The rheological  
 122 parameters for the crust and mantle are presented in Table 1. Melt-depleted lithosphere is com-  
 123 monly assumed to be dehydrated, and therefore more viscous than normal lithosphere [Hirth  
 124 and Kohlstedt, 1996]. A strengthening factor of  $\Delta \eta = 3$  is used in Eqs. (7.7) and (7.8) for the de-  
 125 pleted cratonic mantle lithosphere [Wang *et al.*, 2014], while all other materials have  $\Delta \eta = 1$ .  
 126 Due to the non-linear stress-strain rate relationship used in the non-Newtonian rheology, the  
 127 effective compositional viscosity increase depends on the ambient stress or strain rate. In this  
 128 study, we use a ‘constant strain rate’ value of  $\Delta \eta = 3$ , corresponding to a ‘constant stress’ value  
 129 of  $\Delta \eta^n = 46.8$ , for  $n = 3.5$ . The choice of  $\Delta \eta = 3$  is based on the outcomes of our previous studies  
 130 [Wang *et al.*, 2014; 2015b] and is within the range of acceptable values obtained from laborato-  
 131 ry measurements [Hirth and Kohlstedt, 1996; Karato, 2010; Fei *et al.*, 2013].

132

133 **2.2 Model setup**

134 The computational domain is 400 km deep and 1600 km wide, with initially depleted man-  
 135 tle material located between  $x=200$  and 1400 km, and with a 20-km thick crust. This model set-  
 136 up is illustrated in Fig. 1, together with the mechanical and thermal boundary conditions. A  
 137 free-slip boundary condition is used on the surface, which allows for shortening of the litho-  
 138 sphere. The bottom boundary is open to allow material flow in and out of the model domain, so  
 139 that the deformation of the cratonic root is least affected by the bottom boundary. A velocity  
 140 profile ( $v=V_s$  at the surface), that assumes uniform shear stress and zero net flux, is imposed at  
 141 the side boundaries for a given period (see Fig.1 and below), and moves the lithosphere towards  
 142 the centre of the domain. This process mimics a time-limited tectonic shortening event. We con-  
 143 trol the amount ( $L_s$ ) of the lithosphere flow into the domain from the side boundaries by chang-  
 144 ing the imposed inflow speed  $V_s$  and duration  $t_s$ . The amount/length of lithosphere that flows  
 145 into the domain is counted into the total original length ( $L+L_s$ ) of the lithosphere. During the  
 146 shortening event, the original length of the lithosphere ( $L+L_s$ ) shortens to a length of  $L$ . Then  
 147 the shortening factor of the lithosphere can be calculated after [Mckenzie and Bickle, 1988] as:

148 
$$\beta = \frac{L}{L+L_s} = \frac{L}{L+2 \times V_s \times t_s} \quad (11)$$

149 where  $L=1600\text{km}$  is the width of the model domain.  $\beta = 0.62$  in the Reference Model R  
 150 (see Table 2). Although isostatic balance is implicitly maintained through normal stresses acting  
 151 on the free-slip surface boundary, topography is not explicit in the models. Therefore, surface  
 152 erosion processes are also not considered in this study, which is probably one of the main model  
 153 limitations, since this process might affect crustal thickness over long timescales.

154 We ignore any initial thermal differences between the depleted mantle and normal mantle,  
 155 and use a 30 Myr half-space cooling age for the initial thermal structure of the whole lithosphere,  
 156 as shown in Fig.1. Considering the intense radiogenic heating within continental crust during  
 157 the Archean [Mareschal and Jaupart, 2006], this young thermal age of lithosphere is appropri-  
 158 ate. As we aim to model the thickening of cratonic root in the hotter Archean era, we use an ini-  
 159 tial mantle potential temperature of  $1550^\circ\text{C}$  in the models, which is within the range of petrolog-  
 160 ical estimates [Herzberg *et al.*, 2010, Condie *et al.*, 2016]. The first-order effect of mantle secu-  
 161 lar cooling is included by a constant cooling rate  $\lambda$  ( $^\circ\text{C}/\text{Gyr}$ ) for the basal temperature boundary  
 162 condition:

163 
$$T_b = T_{b0} - \lambda t \quad (12)$$

164 Secular cooling of the Earth's mantle ( $\lambda$ ) has been estimated to be 50-100  $^\circ\text{C}/\text{Gyr}$  [e.g. Grove  
 165 and Parman, 2004; Michaut and Jaupart, 2007; Herzberg *et al.*, 2010]. We use  $\lambda = 100$   $^\circ\text{C}/\text{Gyr}$   
 166 in the reference model, but we also explore the effects of different cooling rates in section 3.2.3.

167 Compositional buoyancy due to melt depletion in the lithospheric mantle plays an im-  
 168 portant role in the presented models. The effect of melt depletion on the mantle density has been  
 169 suggested to be smallest at pressures between 1 and 3 GPa, where 20% melt removal results in

170 only a 0.42% ~0.46% density reduction, compared to 0.90%-1.14% at pressures between 3.5-  
171 4.5 GPa (Fig.1) [Schutt and Lesher, 2006]. The amount of depletion within the lithospheric pro-  
172 file, however, is likely to decrease with depth. We combine these contrasting effects, and assign  
173 an effective compositional density reduction due to melt depletion as shown in Fig1,A2. This  
174 amounts to a maximum density reduction of  $31.5 \text{ kg/m}^3$  (0.95%) in our models, consistent with  
175 experimental data at pressures around 3.5~4.5 GPa [Fig 1,A3, Schutt and Lesher, 2006].

176 Apart from the rheological and density effects of the crust, its high radiogenic heat produc-  
177 tion during the Archean may also play a role in the dynamics of lithospheric shortening. We use  
178 a present-day crustal radiogenic heat production  $Q_0=0.02 \text{ } \mu\text{W/m}^3$ , a constant ratio of 30:1 of the  
179 radiogenic heating between the crust and mantle, and an Archean heat production of 3 times the  
180 present-day value with a half-life of 1.8 Gyr for both the crust and mantle. These values fall  
181 within the suggested ranges for the Earth's thermal evolution and heat production values  
182 [Michaut and Jaupart, 2007; Michaut et al., 2009].

### 183 **3. Results**

#### 184 **3.1 Cratonic thickening processes**

185 Figures. 2 and 3 show the general thickening process of the cratonic root in the Reference Mod-  
186 el R (Table 2) with temperature, composition, velocity and viscosity evolution. Craton thicken-  
187 ing begins with an initial 50 Myr of compressive shortening, but after this period of externally  
188 imposed tectonic shortening, thickening continues, and eventually the initially thin layer of de-  
189pleted mantle material slowly grows into a thick cratonic root over a total duration of several  
190 100 Myrs. At that point, the lithosphere in the model has reached an equilibrium stage, in which  
191 compositional and thermal buoyancy has become similar, and diffusive cooling from the surface  
192 and convective heating at the base of the lithosphere approximately cancel out. To illustrate the  
193 dynamics of this thickening process, the evolution of the depleted root is monitored in several  
194 ways. In Fig.2, the area with  $T>1400^{\circ}\text{C}$  is removed, so that the temperature images effectively  
195 show the (thermally defined) lithosphere. Hereafter, we refer the areas shown in the Fig. 2 by  
196 the temperature image and chemical contour (green) as the thermal root and chemical root, re-  
197 spectively. The thickness of the cratonic root is monitored through time as the average depth  
198 extent of the chemical root in the central region between  $x=550 \text{ km}$  and  $x=1050 \text{ km}$ . We also  
199 calculate the remaining root in the cratonic lithosphere as the percentage of the original root  
200 volume, to monitor the erosion of the root. The time evolution of Reference Model R is shown  
201 in Fig. 4 (red line) in terms of the average chemical root thickness (Fig. 4A) and remaining root  
202 percentage (Fig. 4B).

203 The thickening process consists of two separate stages. The first stage is a direct conse-  
204 quence of the externally imposed compressional tectonic shortening. As constant inward veloci-  
205 ties are imposed at both side boundaries, the depleted root material in the middle of the domain  
206 is pushed downwards, which causes the initial shortening and thickening of the cratonic root

207 (Fig.2A and 3A). As the depleted mantle material is compositionally buoyant and more viscous  
208 compared to normal mantle, it resists this thickening process, which results in more thickening  
209 at the edge than at its interior (Fig. 2A). The depleted root material is thickened from ~130 km  
210 (including the thin transition layer) to about ~173 km depth within the first 50 Myr, while the  
211 thermal root is significantly thinner (Fig. 2A and 3A). After the imposed compressional thicken-  
212 ing of Stage 1, the resultant thermal and chemical structure is by no means in steady state. When  
213 the thickened root cools and becomes denser, its negative thermal buoyancy starts to exceed the  
214 inherent chemical buoyancy and results in further thickening (Stage 2), as shown by the evolu-  
215 tions of i) temperature (Fig.2B-2D), ii) composition (Fig. 3B-3D) and iii) viscosity (Fig. 3F-3H)  
216 evolution. During this phase, the chemical root grows from ~173 km at  $t = 50$  Myr to ~209 km  
217 depth at  $t = 600$  Myr (red line in Fig. 4A), and the thermal root grows to approximately the same  
218 depth as the chemical root (Fig. 2A-C and Fig.3A-C). This self-driven gravitational thickening  
219 is controlled simply by the cooling of the cratonic lithosphere and therefore has a similar time-  
220 scale to that of the thermal diffusive cooling of the lithosphere. Both of the two thickening stag-  
221 es involve some recycling of the root material as illustrated in Fig. 4B (red line): ~20% during  
222 the compressive thickening regime and ~6% during the self-driven thickening regime. The cra-  
223 tonic root continues to slowly thicken and shorten as a result of deformation after 600 Myrs (Fig.  
224 2C-D), but almost no chemical root recycling occurs (Fig.3B). This indicates that the buoyancy  
225 and high viscosity of the now thickened depleted root prevents the development of a significant  
226 Rayleigh-Taylor instability and stabilizes the root during and after the major gravitational thicken-  
227 ing.

## 228 **3.2 Model parameter sensitivity**

229 In order to investigate how robust the results in the Reference Model R are, a series of “sensi-  
230 tivity testing” model calculations are performed, in which some of the most influential model  
231 parameters are varied.

### 232 **3.2.1 Shortening factor**

233 First, the effects of different shortening factors  $\beta$  are investigated, by changing the duration of  
234 shortening and thus the length of the lithosphere that flows into the domain. The same 1cm/yr  
235 inflow speed is imposed at the boundary but with different shortening durations of 0 Myr (SF1),  
236 30 Myr (SF2), 50 Myr (R) and 80Myr (SF3), resulting in respective shortening factors of 1 ,  
237 0.73, 0.62 and 0.5 (Table 2). Fig. 4 illustrates the evolution of the (compositional) thickness and  
238 the remaining root volume in these models. Without any imposed shortening (Model SF1), no  
239 self-driven gravitational thickening of the depleted mantle occurs either (Fig.4A). Although  
240 most of the depleted material survives for at least 1 Gyr in this case (green line in Fig.4B), a  
241 thick cratonic root that approaches the observed thickness of modern-day cratons, is not formed.  
242 In Model SF2 (1cm/yr  $\times$  30 Myr), a slow self-driven thickening stage follows the tectonic  
243 shortening stage and helps to form a lithosphere root with an approximately steady-state depth  
244 of ~160 km (blue line in Fig.4A). However, 160 km is significantly thinner than the thicknesses  
245 of most present-day cratons [e.g. *Gung et al.*, 2003; *Priestley and McKenzie*, 2013]. From Fig.

246 4A, it is clear that the gravitational thickening (Stage 2) is significantly larger in Reference  
247 Model R (~43 km) than in Model SF2 (~10 km). This illustrates that substantial initial thicken-  
248 ing and shortening of depleted lithospheric mantle material is essential for the development of  
249 subsequent late-stage gravitational thickening of the cratonic root.

250 Imposing significantly more shortening than in the reference model leads to different dy-  
251 namics, as shown by Model SF3 (Fig. 4 and 5A-C). In that case, the depleted material is pushed  
252 down to a depth of more than 240 km within 80 Myrs. Late-stage additional thickening does not  
253 occur in this model, but, instead, significant thinning of the root occurs (orange lines in Fig. 4)  
254 due to the fact that the root is too buoyant to stay at the increased depth (unstable structure of  
255 the thick root). The convex upward shape of both the compositional and thermal roots in Fig.  
256 5A illustrates the resistance of the depleted buoyant root against the imposed shortening. As the  
257 root cools down through time, it becomes eroded from the side to the center and the lower ther-  
258 mal and compositional surfaces slowly convert to a convex downward form (Fig. 5B). Unlike in  
259 previous models, the chemical root undergoes significant instability and recycling (Fig.4B and  
260 5A-C) before it has the chance to cool down sufficiently to form a stabilizing thermal boundary,  
261 as it does in Reference Model R. Instead, more and more root material is recycled (orange line  
262 in Fig. 4B) and the root becomes progressively smaller (Fig. 5A-C) over time, which does not  
263 form a stable craton.

### 264 **3.2.2 Shortening rate**

265 Next, we investigate the effects of different shortening rates by imposing the same shortening  
266 amount as in the Reference Model R ( $\beta=0.62$ ). As listed in Table 2, these different shortening  
267 rates lead to shortening durations of 25, 35, 50, 100, and 200 Myrs in models SR1, SR2, R, SR3,  
268 and SR4 (Table 2), respectively. Although the imposed inflow rate varies by about an order of  
269 magnitude among the models, all of these models form a cratonic root of ~200 km or thicker  
270 (Fig.6). Except for Model SR1, the recycling of the root during craton thickening generally  
271 shows a positive correlation with the shortening rate, with slower shortening resulting in less  
272 recycling of the root (Fig. 6B). This is explained by the stress field imposed by the tectonic  
273 shortening. Faster shortening induces stronger stress-weakening effects on the root material,  
274 which, in turn, leads to more delamination of this root. A sudden drop in the amount of remain-  
275 ing root at the end of the tectonic shortening stage in Model SR1 SR2, R, and SR3 in Fig. 6B is  
276 caused by the delamination of root material in these models. This phenomenon does not occur  
277 in Model SR4, which experiences very slow shortening. However, Model SR1, which has the  
278 fastest shortening rate, preserves more root material than most other models and indicates an-  
279 other regime of shortening dynamics, as elaborated below.

280 In order to show the differences in shortening dynamics between the different models, the  
281 chemical root geometry in Models R, SR1 and SR4 is plotted for a model time around 600 Myr  
282 in Fig. 5D-F. Within the shortening time of 25 Myr in Model SR1, part of the root material  
283 starts to delaminate from the main root but has not cooled down enough yet to become suffi-



284 ciently dense to detach completely into the underlying asthenosphere. Instead, it resides at either  
285 side of the main cratonic root, and buffers the main root from edge-driven erosion (Fig.5E),  
286 which prevents it from significant gravitational thickening. The root in the fast shortening Mod-  
287 el SR1 is therefore slightly thinner (Fig.6A), but preserves more root than in the slower-  
288 shortening Models SR2, R, or SR3 (Fig. 6B). On the other hand, Model SR4, with the slowest  
289 shortening rate, preserves almost 95% of its original depleted mantle area without any sudden  
290 losses of root material (Fig.6B). In this case, the root has enough time to cool down, and stress  
291 weakening induced by tectonic-shortening is insufficient to delaminate any significant amount  
292 of root material. These results illustrate that the tectonically induced shortening rate during cra-  
293 ton formation plays an important role in the thickening dynamics and the recycling of the cra-  
294 tonic root.

### 295 **3.2.3 Secular cooling**

296 In our Reference Model *R*, the basal temperature reduces by  $100^{\circ}\text{C}/\text{Gyr}$  in order to mimic the  
297 effects of secular cooling of the mantle. In this section, we compare models with different cool-  
298 ing rates (Table 2) and show how this affects the craton thickening and stabilization process. Fig.  
299 7 shows the thickness and root volume evolution of three models with cooling rates of  
300  $100^{\circ}\text{C}/\text{Gyr}$  (Model *R*),  $50^{\circ}\text{C}/\text{Gyr}$  (Model *SC1*), and  $0^{\circ}\text{C}/\text{Gyr}$  (i.e. no cooling, Model *SC2*).  
301 While Models *R* and *SC1* remain stable even after  $t = 1$  Gyr, *SC2* without basal cooling  
302 ( $0^{\circ}\text{C}/\text{Gyr}$ ) has a quiet period until  $t=1$ Gyr, but then starts to show significant perturbations as  
303 observed in both the root thickness (Fig. 7A) and root volume (Fig. 7B). The cratonic root is  
304 clearly thinned and recycled during this active period, indicating substantial root dynamics. The  
305 average velocity of the compositional root (Fig. 7C) shows that the cratonic root in Model *SC2*  
306 becomes dynamically active after 1 Gyr, such that it approaches the average velocity of the  
307 whole computational domain (thick, red). The root in Model *R* becomes less active (and thus  
308 more stable) over the same time period, while the root in Model *SC1* ( $50^{\circ}\text{C}/\text{Gyr}$ ) displays a rela-  
309 tively constant degree of activity through time.

310 To further illustrate the nature of the instabilities in Model *SC2*, its root dynamics are moni-  
311 tored and illustrated over a short 36-Myr timespan from 1409 to 1445 Myr (Fig.8). The core of  
312 the root displays minimal change of shape within this short period, as indicated by the isotherms  
313 ( $1100^{\circ}\text{C} - 1300^{\circ}\text{C}$ ). However, during this period, some of the marginal root material vigorously  
314 moves around cyclically in a timescale of 30-40 Myrs. Each cycle results in some of the root  
315 material eroding away (Fig.8B). Unlike a more classical Rayleigh-Taylor instability of the  
316 thickening lithosphere [*Houseman and Molnar, 1997*] in which the root material typically never  
317 returns, this instability of the compositionally buoyant root shows an oscillatory behaviour.  
318 Similar oscillatory instabilities were also found in both laboratory studies [e.g. *Jaupart et al.,*  
319 *2007*] and independent numerical modelling studies [e.g. *Y.Wang et al., 2015*].

320

## 321 **4 Discussion**

322 Our numerical models show that craton roots of similar thickness to Earth's cratons (>200 km)  
323 can be formed successfully from a relatively thin depleted mantle lithosphere layer (30-120 km),  
324 through a two-stage thickening and stabilization process. The starting thickness is no greater  
325 than the thickness of depleted buoyant oceanic lithosphere expected to form at a hot mid-ocean  
326 ridge for instance [e.g., Herzberg et al., 2010]. In this scenario, cratonization is triggered by tec-  
327 tonic shortening, which is then followed by a period of internally-driven gravitational thicken-  
328 ing, as illustrated in Fig.9. Significant downward movement and cooling of cratonic root mate-  
329 rial occurs during craton formation, a result that is consistent with the observation that cratons  
330 are typically thicker and colder than its protolith [Lee and Chin, 2014]. Below, we further dis-  
331 cuss the viability and limitations of this cratonization model in relation to two important aspects:  
332 craton formation and craton stabilization.

### 333 **4.1 Formation of cratons**

334 The initial, tectonically driven, compressive thickening phase in our proposed cratonization pro-  
335 cess plays an essential role in the initialization of the thickening process (Fig. 9). Without  
336 enough initial compressive thickening of the depleted mantle material, the subsequent self-  
337 driven thickening of the root will not take place (Model SF1) or cannot form a substantial cra-  
338 tonic root (Model SF2). However, thickening is not necessarily achieved by the simple shorten-  
339 ing process that is used in this study. *Sleep* [2005] suggested that cratonic lithosphere is formed  
340 by processes analogous to modern tectonics. Indeed, cratonization might involve phenomena  
341 such as subduction accretion, lithospheric underplating, or continental collision, all of which  
342 require tectonic, localised deformation, processes that are not accurately captured by our rela-  
343 tively simple model setup. Studies of modern collision tectonics have shown that the plate con-  
344 vergence is accommodated by a variety of mechanisms [Toussaint et al., 2004; Burov and  
345 Yamato, 2008], including shortening by pure-shear thickening or folding. The most striking,  
346 present-day example of this is the formation of the Tibetan plateau, whose lithosphere has un-  
347 dergone several hundred kilometres of shortening over 10s of Myr [DeCelles, 2002; Tian et al.,  
348 2013]. McKenzie & Priestly (2016) have recently proposed that the Tibetan Plateau and its un-  
349 derlying root is the best modern example of a craton in the early stages of its formation. Wheth-  
350 er the Tibetan plateau will eventually form a stable craton or not under the present-day mantle  
351 conditions is beyond the scope of this study, but it provides a real example of the time and  
352 length scales of compressive thickening as envisioned in our models. Regardless of the tectonic  
353 manifestation, craton formation requires lithosphere to gradually develop strength and a balance  
354 between compositional and thermal buoyancies such that deformable lithosphere can grow into  
355 virtually indestructible cratons.

356 Although our models show that the slow, prolonged tectonic shortening preserves more  
357 cratonic root than fast, short-lived tectonic thickening (Fig.6), compressive shortening events  
358 lasting 100s of Myr (Models SR3 and SR4) are not documented in the geological record. This

359 suggests that fast, short-lived shortening (10s of Myr, e.g., Models SR1,SR2 and R) that involve  
360 substantial recycling (~30%) of the root probably provides a more realistic craton formation  
361 scenario, especially in the Archean Earth where plate speeds could have been faster [*van Hunen*  
362 *and van den Berg*, 2008]. The high stresses associated with the rapid shortening of Model SR1  
363 lead to significant localized yielding of the lithosphere, and the associated localized crustal  
364 thickening induces an undulating boundary on the top of the root (Fig.5E). This behaviour is  
365 similar to that described for the localized thickening of cratonic lithosphere by *Cooper and*  
366 *Miller* [ 2014], who proposed that the variable depth of the observed mid-lithospheric seismic  
367 discontinuities within cratonic lithosphere might be introduced by the thickening phase during  
368 the craton formation.

369         Therefore, we propose a two-stage development of cratons, wherein the second stage -  
370 gravitational thickening - lasts for 100s of Myr (Fig. 6), and is driven by the cooling and growth  
371 of the negative thermal buoyancy of the root material as a result of the compressive thickening  
372 and subsequent diffusive cooling. *Mareschal and Jaupart* [2006] suggested that the thermal  
373 field of cratonic lithosphere might remain in disequilibrium for ~1-2 Gyrs after root formation,  
374 which is broadly consistent with the ~600 Myrs of continued thickening displayed by our mod-  
375 els as result of the thermal adjustment. This thermal adjustment also helps to stabilize the cra-  
376 tonic root, as discussed below. The thickening speed during this latter stage of craton evolution  
377 is significantly lower than in the first thickening stage as there is no external shortening imposed.  
378 Nonetheless, the cratonic root grows vertically by ~40 km during stage-2 thickening in our Ref-  
379 erence Model R (Fig.4), compared with ~43 km stage-1 thickening. This suggests that the two  
380 thickening stages may contribute equally to the total overall thickness of the cratonic lithosphere.  
381 The vertical movement of cratonic mantle material, which is implicit in these models, may be a  
382 way to generate specific aspects of the mineralogy of cratons, such as the presence of high-Cr,  
383 low-Ca knorringitic garnets that require low-pressure (<3GPa) depleted precursor lithologies  
384 that become subsequently pressurized to ~4 to 7 GPa [*Canil and Wei*, 1992; *Stachel et al.*, 1998].

#### 385 **4.2 Stabilization of cratons**

386 Even though the high intrinsic viscosity and chemical buoyancy of the depleted root play im-  
387 portant roles in the long-term stability of the cratons, our models show that the presence of a  
388 large amount of depleted mantle beneath continental crust material does not guarantee a stable  
389 craton. In the Reference Model R, the gravitational thickening stage is driven by the diffusive  
390 cooling of the root, and slowly embeds the chemically depleted root material within the thermal  
391 lithosphere, leading to a stable cratonic root (Fig. 2 C-D). But if significantly more initial, tec-  
392 tonic shortening is applied (e.g. in Model SF3), the cratonic root (Fig. 4A) does not stabilize,  
393 and experiences continuous, significant basal erosion, even after long cooling periods. Therefore,  
394 rapid compressive shortening (10s of Myr) of a depleted mantle lithosphere alone may not form  
395 a stable thermo-chemical structure. Instead, a slow self-driven thickening and adjustment pro-  
396 cess, as a result of thermal equilibration [*Schutt and Leshner*, 2006], is required to stabilize the

397 newly formed cratonic root. Within the context of our model parameters, the thickness of cra-  
398 tonic roots can be self-regulating and such a process may explain the relatively constant thick-  
399 ness of present-day cratonic roots.

400       Apart from an instability caused by large-scale tectonic shortening, our model results also  
401 illustrate another type of instability that can occur, as illustrated by Model SC2. In that case,  
402 cratonic root material becomes unstable and starts to oscillate on a timescale of a 10s of Myrs  
403 (Fig. 8). Such oscillatory behaviour occurs after an initial, long quiet period of ~1.1 Gyr (Model  
404 SC2 in Fig. 7). This type of instability has previously been observed in other studies [*Jaupart et*  
405 *al.*, 2007; *Y.Wang et al.*, 2015], and is different from a more commonly reported Rayleigh-  
406 Taylor style root collapse [e.g. *Houseman and Molnar*, 1997]. A possible geological expression  
407 of this type of instability might be the complex temporal additions/modification of cratonic roots  
408 indicated by Re-Os isotopes and petrological studies of mantle xenoliths from the Rae craton,  
409 which appears to have experienced a considerably more complex evolutionary history than most  
410 cratons [*Liu et al.*, 2016]. Secular cooling is able to prevent the system from developing this  
411 oscillatory regime due to a combination of two effects. Firstly, the buoyancy number (ratio be-  
412 tween the compositional buoyancy and thermal buoyancy) is increased by reducing the tempera-  
413 ture contrast during secular cooling. Secondly and perhaps more importantly, the Rayleigh  
414 number of the mantle convection is reduced as a result of the increase of background viscosity  
415 due to mantle cooling. Both of the two effects contribute to switching the system into a stable  
416 regime and leads to the stabilization of the cratonic root.

417       As a result of its long-term thermal evolution, a cratonic root that is approximately iso-  
418 pycnic under present conditions would have been either more or less buoyant in the past [*Eaton*  
419 *and Perry*, 2013]. This indicates that the long-term stability of cratons cannot simply be ex-  
420 plained by a permanently isopycnic status, and that other contributions, for example from the  
421 high viscosity of the root [e.g. *Wang et al.*, 2014] or secular cooling [*Michaut et al.*, 2009], are  
422 essential to explain long-term cratonic root stability. On the basis of laboratory studies of the  
423 effects of melt depletion on the physical properties, *Schutt and Lesher* [2006] proposed another  
424 possible stabilization mechanism for cratons. Their experimental data argue that the depletion  
425 induced buoyancy for cratonic mantle that formed above 110 km is not enough to counteract the  
426 negative thermal buoyancy at their formation depth. Instead, the neutral buoyancy of the craton-  
427 ic root might be achieved through thermal re-equilibrium after vertical transportation of the cra-  
428 tonic mantle and through thermal expansivity variation due to temperature and pressure changes.  
429 Such an effect, if taken into account in the geodynamical modelling, would potentially further  
430 promote the thickening and stabilization of cratonic root.

431       The models presented here have implications for the topographical evolution of cratons  
432 and their roots. In their early evolution, cratons witnessed dramatic subsidence, with the devel-  
433 opment, in some cases, of very large sedimentary basins, e.g., the 8 km thick Meso- to Neoar-  
434 chean Witwatersrand basin of the central Kaapvaal craton [*Robb & Meyer*, 1995]. McKenzie &

435 Priestley (2016) have argued that the formation of intra-cratonic basins is a specific outcome of  
436 the thickening phase of cratons by lateral compression, if thick crust exists for a timescale on  
437 the order of the thermal time constant of thick lithosphere and is then subsequently rapidly re-  
438 moved by erosion. In this sense, the lack of ability of our models to examine in detail the sur-  
439 face processes and crustal evolution accompanying craton formation are a weakness. The sur-  
440 face of the model domain is free-slip, which does not allow vertical motion as a response to  
441 mantle dynamics, and erosion and sedimentation processes are not considered. Also prograde  
442 metamorphism and densification of crust are not considered, so that delamination of eclogitic  
443 crust [e.g. Pearson & Wittig, 2008] does not occur. For now, the reader is referred to McKenzie  
444 & Priestley [2016] for a more detailed examination of the behavior of the crust. Our models,  
445 instead, focus on the mantle part of the lithosphere as this portion is essential in maintaining the  
446 overall long-term integrity of a craton. To compensate for the secondary processes that tend to  
447 reduce crustal thickness, our models start with a relatively thin (20 km) crust. The crust forms  
448 only a relatively small fraction of the total craton, and we do not expect its effects on craton keel  
449 root development and underlying mantle dynamics to be significant. The complex metamorphic  
450 and structural evolution of young cratons are difficult to explore in our models in which topog-  
451 raphy can only be approximated through normal stresses on the top boundary. Evaluating the  
452 level of consistency between our models and these observations requires a detailed evaluation of  
453 the impact of the varying parameters in the models that will be explored elsewhere.

## 454 **5 Conclusion**

455 We performed numerical experiments to study the thickening and stabilization of cratonic roots  
456 in a thermally evolving mantle to explore a compressive thickening model for making thick cra-  
457 tonic roots (Jordan, 1978; McKenzie & Priestley, 2016). Our modelling results show a two-  
458 stage thickening and stabilization process, in which a layer of depleted mantle (30-120 km)  
459 forms a thick cratonic root (>200 km) within in a few 100 Myr. This process involves signifi-  
460 cant vertical movement of cratonic mantle material as an intrinsic part of the cratonization pro-  
461 cess, which agrees well with petrological observations [Canil & Wei, 1992; Lee and Chin, 2014]  
462 and geophysical arguments [Schutt and Lesher, 2006]. Based on the geodynamical modelling,  
463 we suggest the following related key ingredients for the cratonization process: 1. Thickening of  
464 the cratonic root is initiated by a tectonic shortening phase that lasts for 10s of Myr and is fol-  
465 lowed by a gravitational thickening phase that lasts for 100s of Myr. 2. Initial tectonic shorten-  
466 ing and thickening of previously depleted material occurs on length and time scales similar to  
467 modern orogenic tectonics (e.g. subduction accretion, lithosphere underplating, or continental  
468 collision), and is essential to initiate the cratonization process. 3. Gravitational self-thickening  
469 always follows initial tectonic compressive shortening and causes further thickening, while in-  
470 trinsic compositional buoyancy prevents a Rayleigh-Taylor type collapse, and stabilizes the  
471 thick cratonic root. 4. Secular cooling of the ambient mantle has a stabilizing effect on the cra-  
472 tonic root by reducing the thermal buoyancy contrast between lithosphere and asthenosphere

473 and increasing background viscosity, and forms an essential ingredient for the long-term surviv-  
474 al of cratons.

475

476 **Acknowledgements:**

477 We would like to thank Thomas François, an anonymous reviewer, the editor and guest editor  
478 for their constructive comments that helped to significantly improve the manuscript. We also  
479 thank Yaoling Niu for useful discussions. The data for this paper are available by contacting the  
480 corresponding author. The work has been supported by EU FP7 Marie Curie Initial Training  
481 Network 'Topomod' contract 264517. J.v.H. acknowledges funding from the European Re-  
482 search Council (ERC StG279828) and D.G.P. was supported by a Canada Excellence Research  
483 Chair.

484 **Bibliography**

- 485 Condie, K.C., Aster, R.C. & van Hunen, J. (2016). A great thermal divergence in the mantle  
486 beginning 2.5 Ga: Geochemical constraints from greenstone basalts and komatiites. *Geo-*  
487 *science Frontiers* 7(4): 543-553.
- 488 Arndt, N. T., N. Coltice, H. Helmstaedt, and M. Gregoire (2009), Origin of Archean  
489 subcontinental lithospheric mantle: Some petrological constraints, *Lithos*, 109(1-2), 61–71,  
490 doi:10.1016/j.lithos.2008.10.019.
- 491 Aulbach, S. (2012), Craton nucleation and formation of thick lithospheric roots, *Lithos*, 149,  
492 16–30, doi:10.1016/j.lithos.2012.02.011.
- 493 B élard, J. H., P. Brouillette, L. Madore, and A. Berclaz (2003), Archaean cratonization and  
494 deformation in the northern Superior Province, Canada: An evaluation of plate tectonic  
495 versus vertical tectonic models, *Precambrian Res.*, 127(1-3), 61–87, doi:10.1016/S0301-  
496 9268(03)00181-5.
- 497 Burov, E., and P. Yamato (2008), Continental plate collision, P-T-t-z conditions and unstable vs.  
498 stable plate dynamics: Insights from thermo-mechanical modelling, *Lithos*, 103(1-2), 178–  
499 204, doi:10.1016/j.lithos.2007.09.014.
- 500 Burov, E. B. (2011), Rheology and strength of the lithosphere, *Mar. Pet. Geol.*, 28(8), 1402–  
501 1443, doi:10.1016/j.marpetgeo.2011.05.008.
- 502 Canil, D. (2004), Mildly incompatible elements in peridotites and the origins of mantle  
503 lithosphere, *Lithos*, 77, 375–393, doi:10.1016/j.lithos.2004.04.014.
- 504 Canil, D., and K. Wei (1992), Constraints on the origin of mantle-derived low Ca garnets,  
505 *Contrib. to Mineral. Petrol.*, 109(4), 421–430, doi:10.1007/BF00306546.
- 506 Carlson, R. R. W., D. G. Pearson, and D. D. E. James (2005), Physical, chemical, and  
507 chronological characteristics of continental mantle, *Rev. Geophys.*, (2004), 1–24,  
508 doi:10.1029/2004RG000156.
- 509 Cooper, C. M., and M. S. Miller (2014), Craton formation: Internal structure inherited from  
510 closing of the early oceans, *Lithosphere*, 6(1), 35–42, doi:10.1130/L321.1.
- 511 DeCelles, P. G. (2002), Implications of shortening in the Himalayan fold-thrust belt for uplift of  
512 the Tibetan Plateau, *Tectonics*, 21(6), doi:10.1029/2001TC001322.
- 513 Eaton, D. W., and H. K. Claire Perry (2013), Ephemeral isopycnicity of cratonic mantle keels,  
514 *Nat. Geosci.*, 6(11), 967–970, doi:10.1038/ngeo1950.

## Bibliography

- 515 Fei, H., M. Wiedenbeck, D. Yamazaki, and T. Katsura (2013), Small effect of water on upper-  
516 mantle rheology based on silicon self-diffusion coefficients, *Nature*, 498(7453), 213–215,  
517 doi:10.1038/nature12193.
- 518 Griffin, W. L., S. Y. O'Reilly, N. Abe, S. Aulbach, R. M. Davies, N. J. Pearson, B. J. Doyle,  
519 and K. Kivi (2003), The origin and evolution of Archean lithospheric mantle, in  
520 *Precambrian Research*, vol. 127, pp. 19–41.
- 521 Grove, T. L., and S. W. Parman (2004), Thermal evolution of the Earth as recorded by  
522 komatiites, *Earth Planet. Sci. Lett.*, 219, 173–187, doi:10.1016/S0012-821X(04)00002-0.
- 523 Gung, Y., M. Panning, and B. Romanowicz (2003), Global anisotropy and the thickness of  
524 continents, *Nature*, 422(April), 707–711, doi:10.1038/nature01557.1.
- 525 Herzberg, C. (1999), Phase equilibrium constraints on the formation of cratonic mantle, in  
526 *Mantle Petrology: Field Observations and High-Pressure Experimentation. Spec. Publ.*  
527 *Geochem. Soc. No. 6*, pp. 241–257.
- 528 Herzberg, C., K. Condie, and J. Korenaga (2010), Thermal history of the Earth and its  
529 petrological expression, *Earth Planet. Sci. Lett.*, 292(1-2), 79–88,  
530 doi:10.1016/j.epsl.2010.01.022.
- 531 Hirth, G., and D. L. Kohlstedt (1996), Water in the oceanic upper mantle: implications for  
532 rheology, melt extraction and the evolution of the lithosphere, *Earth Planet. Sci. Lett.*,  
533 144(1-2), 93–108.
- 534 Hirth, G., R. L. Evans, and A. D. Chave (2000), Comparison of continental and oceanic mantle  
535 electrical conductivity: Is the Archean lithosphere dry?, *Geochemistry, Geophys.*  
536 *Geosystems*, 1(12), DOI: 10.1029/2000GC000048, doi:10.1029/2000GC000048.
- 537 Houseman, G. a., and P. Molnar (1997), Gravitational (Rayleigh-Taylor) instability of a layer  
538 with non-linear viscosity and convective thinning of continental lithosphere, *Geophys. J.*  
539 *Int.*, 128(1), 125–150, doi:10.1111/j.1365-246X.1997.tb04075.x.
- 540 van Hunen, J., and M. B. Allen (2011), Continental collision and slab break-off: A comparison  
541 of 3-D numerical models with observations, *Earth Planet. Sci. Lett.*, 302(1-2), 27–37,  
542 doi:10.1016/j.epsl.2010.11.035.
- 543 van Hunen, J., and A. P. van den Berg (2008), Plate tectonics on the early Earth: Limitations  
544 imposed by strength and buoyancy of subducted lithosphere, *Lithos*, 103(1-2), 217–235,  
545 doi:10.1016/j.lithos.2007.09.016.
- 546 van Hunen, J., S. Zhong, N. M. Shapiro, and M. H. Ritzwoller (2005), New evidence for  
547 dislocation creep from 3-D geodynamic modeling of the Pacific upper mantle structure,  
548 *Earth Planet. Sci. Lett.*, 238, 146 – 155, doi:10.1016/j.epsl.2005.07.006.



## Bibliography

- 549 Jaupart, C., P. Molnar, and E. Cottrell (2007), Instability of a chemically dense layer heated  
550 from below and overlain by a deep less viscous fluid, *J. Fluid Mech.*, 572, 433,  
551 doi:10.1017/S0022112006003521.
- 552 Jordan, T. (1975), The continental tectosphere, *Rev. Geophys.*, 13(3).
- 553 Jordan, T. H. (1978), Composition and development of the continental tectosphere, *Nature*,  
554 274(5671), 544–548, doi:10.1038/274544a0.
- 555 Karato (2010), Rheology of the deep upper mantle and its implications for the preservation of  
556 the continental roots: A review, *Tectonophysics*, 481(1-4), 82–98,  
557 doi:10.1016/j.tecto.2009.04.011.
- 558 Lee, C.-T. A. (2006), Geochemical/Petrologic constraint on the origin of cratonic mantle,  
559 *Geophys. Monogr. - Am. Geophys. union*, 164, 89–114, doi:10.1029/164gm08.
- 560 Lee, C.-T. a., and E. J. Chin (2014), Calculating melting temperatures and pressures of  
561 peridotite protoliths: Implications for the origin of cratonic mantle, *Earth Planet. Sci. Lett.*,  
562 403, 273–286, doi:10.1016/j.epsl.2014.06.048.
- 563 Lee, C.-T. A., P. Luffi, and E. J. Chin (2011), Building and Destroying Continental Mantle,  
564 *Annu. Rev. Earth Planet. Sci.*, 39(1), 59–90, doi:10.1146/annurev-earth-040610-133505.
- 565 Mareschal, J. C., and C. Jaupart (2006), Archean thermal regime and stabilization of the cratons,  
566 in *Archean Geodynamics and Environments*, vol. 164, pp. 61–73.
- 567 McKenzie, D., and M. J. Bickle (1988), The volume and composition of melt generated by  
568 extension of the lithosphere, *J. Petrol.*, 29(3), 625–679, doi:10.1093/petrology/29.3.625.
- 569 McKenzie, D., and K. Priestley (2016), Speculations on the formation of cratons and cratonic  
570 basins, *Earth Planet. Sci. Lett.*, 435, 94–104, doi:10.1016/j.epsl.2015.12.010.
- 571 Michaut, C., and C. Jaupart (2007), Secular cooling and thermal structure of continental  
572 lithosphere, *Earth Planet. Sci. Lett.*, 257(1-2), 83–96, doi:10.1016/j.epsl.2007.02.019.
- 573 Michaut, C., C. Jaupart, and J.-C. Mareschal (2009), Thermal evolution of cratonic roots, *Lithos*,  
574 109(1-2), 47–60, doi:10.1016/j.lithos.2008.05.008.
- 575 Moresi, L.-N., and V. S. Solomatov (1995), Numerical investigation of 2D convection with  
576 extremely large viscosity variations, *Phys. Fluids*, 7(9), 2154–2162, doi:10.1063/1.868465.
- 577 Pearson, D. ., R. W. Carlson, S. B. Shirey, F. R. Boyd, and P. H. Nixon (1995), Stabilisation of  
578 Archaean lithospheric mantle : A Re-Os isotope study of peridotite xenoliths from the  
579 Kaapvaal craton, *Earth Planet. Sci. Lett.*, 134, 341–357.
- 580 Pearson, D. G., and N. Wittig (2014), The Formation and Evolution of Cratonic Mantle  
581 Lithosphere - Evidence from Mantle Xenoliths, in *Treatise on Geochemistry: Second*  
582 *Edition*, vol. 3, pp. 255–292, Elsevier Ltd.

## Bibliography

- 583 Pearson, D. G. D., and N. Wittig (2008), Formation of Archaean continental lithosphere and its  
584 diamonds: the root of the problem, *J. Geol. Soc. London.*, 165(5), 895–914,  
585 doi:10.1144/0016-76492008-003.
- 586 Priestley, K., and D. McKenzie (2013), The relationship between shear wave velocity,  
587 temperature, attenuation and viscosity in the shallow part of the mantle, *Earth Planet. Sci.*  
588 *Lett.*, 381, 78–91, doi:10.1016/j.epsl.2013.08.022.
- 589 Rudnick, R. L., and A. A. Nyblade (1999), The thickness and heat production of Archean  
590 lithosphere: constraints from xenolith thermobarometry and surface heat flow, in *Mantle*  
591 *Petrology: Field Observations and High-Pressure Experimentation. Spec. Publ. Geochem.*  
592 *Soc. No. 6*, vol. 6, pp. 3–12.
- 593 Schubert, G., D. Stevenson, and P. Cassen (1980), Whole planet cooling and the radiogenic heat  
594 source contents of the earth and moon, , 85, 2531–2538, doi:10.1029/JB085iB05p02531.
- 595 Schutt, D. L., and C. E. Leshar (2006), Effects of melt depletion on the density and seismic  
596 velocity of garnet and spinel lherzolite, *J. Geophys. Res.*, 111(B5), B05401,  
597 doi:10.1029/2003JB002950.
- 598 Sizova, E., T. Gerya, K. St üwe, and M. Brown (2015), Generation of felsic crust in the Archean:  
599 A geodynamic modeling perspective, *Precambrian Res.*, 271, 198–224,  
600 doi:10.1016/j.precamres.2015.10.005.
- 601 Sleep, N. H. (2005), Evolution of the Continental Lithosphere, *Annu. Rev. Earth Planet. Sci.*,  
602 33(1), 369–393, doi:10.1146/annurev.earth.33.092203.122643.
- 603 Stachel, T., K. S. Viljoen, G. Brey, and J. W. Harris (1998), Metasomatic processes in  
604 lherzolic and harzburgitic domains of diamondiferous lithospheric mantle: REE in  
605 garnets from xenoliths and inclusions in diamonds, *Earth Planet. Sci. Lett.*, 159(1-2), 1–12,  
606 doi:10.1016/S0012-821X(98)00064-8.
- 607 Tian, X., Z. Liu, S. Si, and Z. Zhang (2013), The crustal thickness of NE Tibet and its  
608 implication for crustal shortening, *Tectonophysics*, 634, 198–207,  
609 doi:10.1016/j.tecto.2014.07.001.
- 610 Toussaint, G., E. Burov, and L. Jolivet (2004), Continental plate collision: Unstable vs. stable  
611 slab dynamics, *Geology*, 32(1), 33–36, doi:10.1130/G19883.1.
- 612 Wang, H., J. van Hunen, D. G. Pearson, and M. B. Allen (2014), Craton stability and longevity:  
613 The roles of composition-dependent rheology and buoyancy, *Earth Planet. Sci. Lett.*, 391,  
614 224–233, doi:10.1016/j.epsl.2014.01.038.
- 615 Wang, H., J. van Hunen, and D. Graham Pearson (2015a), The thinning of subcontinental  
616 lithosphere: The roles of plume impact and metasomatic weakening, *Geochemistry,*  
617 *Geophys. Geosystems*, n/a–n/a, doi:10.1002/2015GC005784.

## Bibliography

- 618 Wang, Y., J. Huang, and S. Zhong (2015b), Episodic and Multi-staged Gravitational Instability  
619 of Cratonic Lithosphere and its Implications for Reactivation of the North China Craton,  
620 *Geochemistry Geophys. Geosystems*, 815–833, doi:doi: 10.1002/2014GC005681.
- 621 Wittig, N., D. G. Pearson, M. Webb, C. J. Ottley, G. J. Irvine, M. Kopylova, S. M. Jensen, and  
622 G. M. Nowell (2008), Origin of cratonic lithospheric mantle roots : A geochemical study  
623 of peridotites from the North Atlantic Craton , West Greenland, *Earth Planet. Sci. Lett.*,  
624 274, 24–33, doi:10.1016/j.epsl.2008.06.034.
- 625 Zhong, S., M. T. Zuber, L. Moresi, and G. Michael (2000), Role of temperature-dependent  
626 viscosity and surface plates in spherical shell models of mantle convection, *J. Geophys.*  
627 *Res.*, 105(B5), 11063–11082, doi:10.1029/2000JB900003.
- 628
- 629

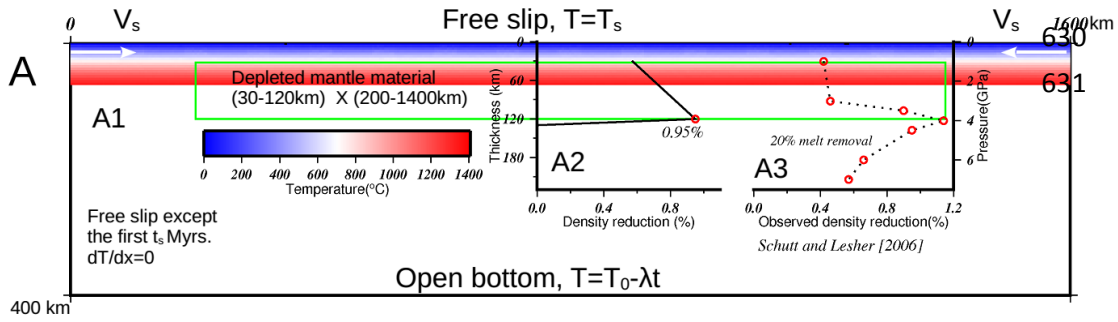


Fig. 1:

632 Model setup of the cratonic root, including mechanical and thermal boundary conditions, initial thermal  
 633 condition and initial chemical profile. The initial compositional profile  $C_2$  (depletion related), as plotted  
 634 in the left inset diagram A2, increases from 0.6 to 1 between 30 km and 120km. The chemical buoyancy  
 635 reaches its maximum value at 120 km, where it is 0.95% less dense than typical the  $3300 \text{ kg/m}^3$  reference  
 636 density for undepleted peridotite. For comparison, the depth-dependent depletion effect for 20% melting  
 637 on the density of mantle peridotite from [Schutt and Leshner, 2006] is plotted in the right inset diagram A3.

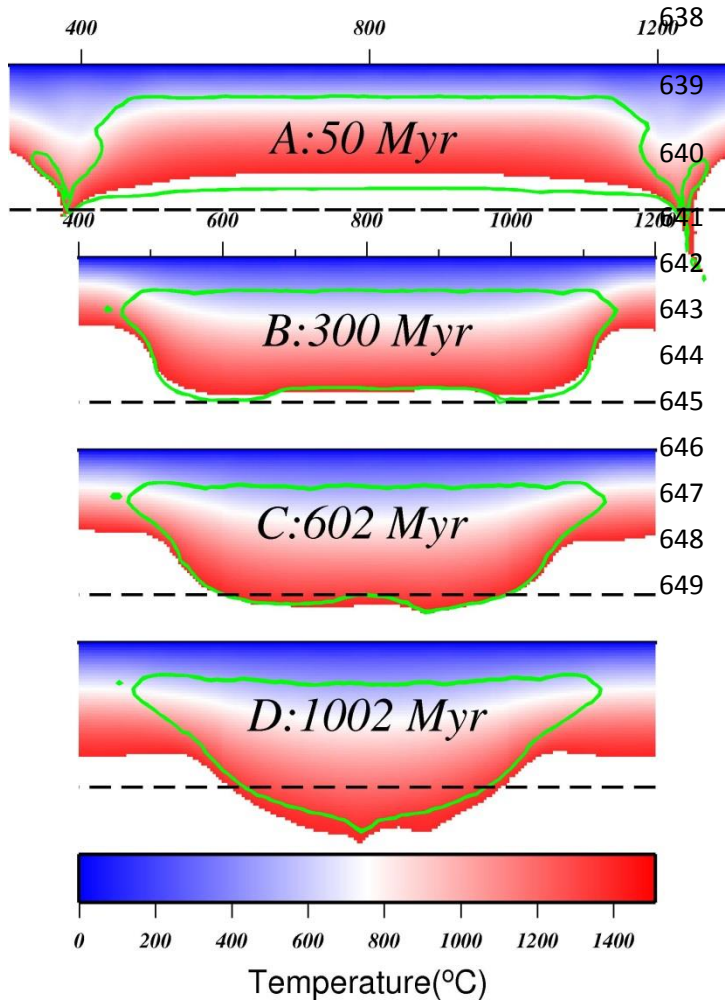
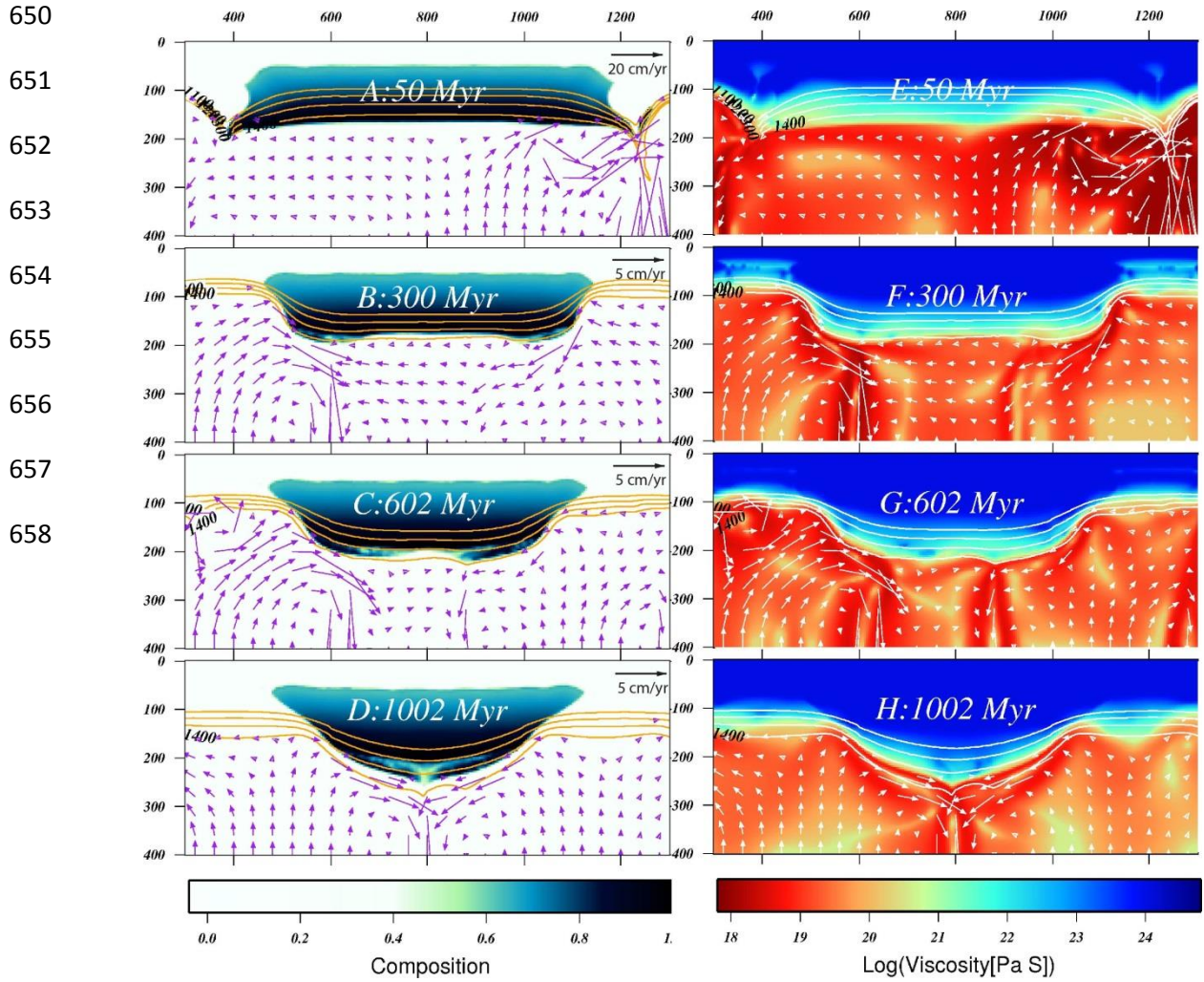
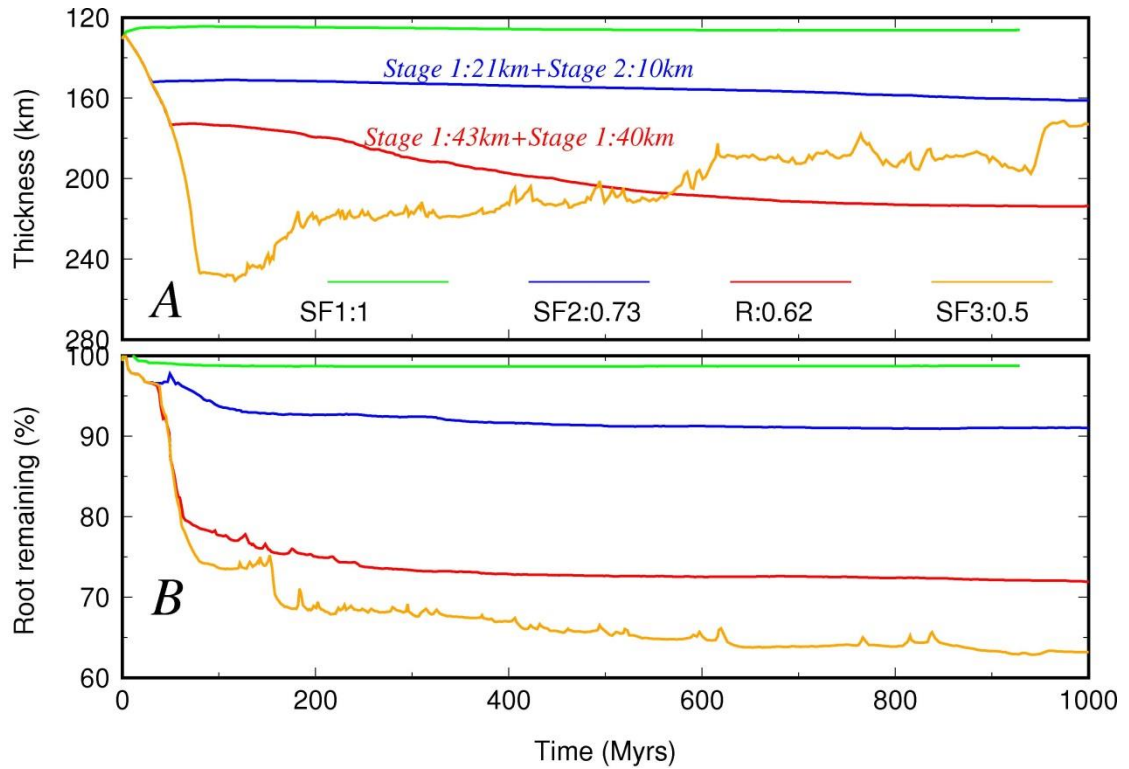


Fig. 2: The thickening process of the cratonic root in Reference Model R. Colours indicate the temperature distribution. Temperatures above  $1400^\circ\text{C}$  (taken as the 'thermal lithosphere boundary in this study) are removed to clarify the lithosphere thickening process. The green contours outline the chemical roots.



659 **Fig. 3:** The evolutions of the chemical root (A-D) and viscosity (E-H) during the thickening process of  
 660 the cratonic c root in Fig. 2. The arrows show the velocity field at each time point. The isotherms of  
 661  $T=1100^{\circ}C$ ,  $1200^{\circ}C$ ,  $1300^{\circ}C$ ,  $1400^{\circ}C$  are also plotted.

662  
 663  
 664  
 665  
 666  
 667



668

669 **Fig. 4:** A) Secular evolution of modelled cratonic roots, measured as their average thickness between  
 670  $x=550$  km and  $x=1050$  km in models with different shortening factor  $\beta$ . The thickness is calculated by  
 671 using the compositional (rather than thermal) root definition in order to exclude any effects of secular  
 672 cooling. The two thickening stages in Model R and SF2, tectonic compressive thickening and gravita-  
 673 tional thickening, are clearly marked by a kink in the curves. B) Volumetric percentage of remaining root  
 674 material over time to illustrate the amount of recycling into the underlying upper mantle of chemical root  
 675 material.

676

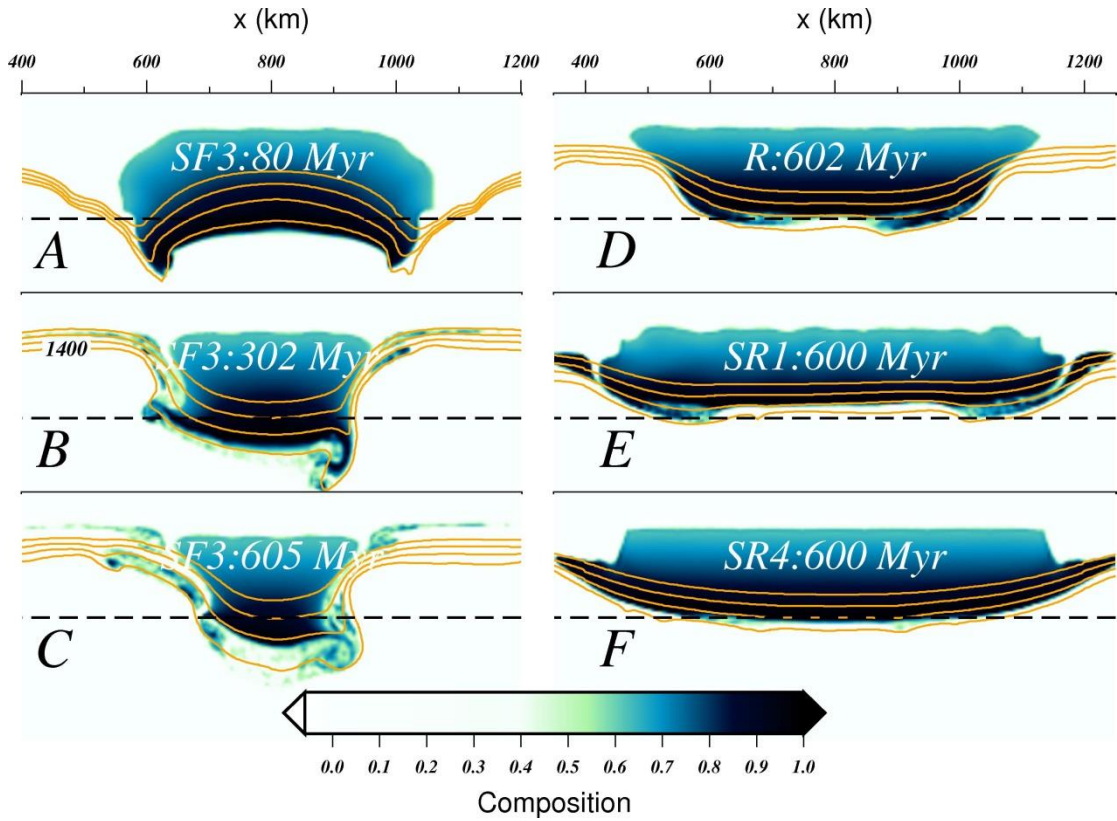
677

678

679

680

681



682

683 **Fig. 5:** A)-C) Chemical root images of Model SF3 at 80Myr (A), 302 Myr (B),605 Myr (C). Significantly  
 684 more tectonic shortening Stage 1) leads to an unstable thermo-chemical structure, in which the root be-  
 685 comes smaller over time. D)-F) Chemical root image of Model R (D), SR1(E) and SR4 (F) at around 600  
 686 Myr. Strong yielding in Model SR1 (E) induces an undulating boundary at the top of the chemical root.  
 687 The orange curves are the isotherm of  $T=1100^{\circ}\text{C}$ ,  $1200^{\circ}\text{C}$ ,  $1300^{\circ}\text{C}$ ,  $1400^{\circ}\text{C}$ , respectively. The dashed  
 688 lines indicate depth intervals of 200 km.

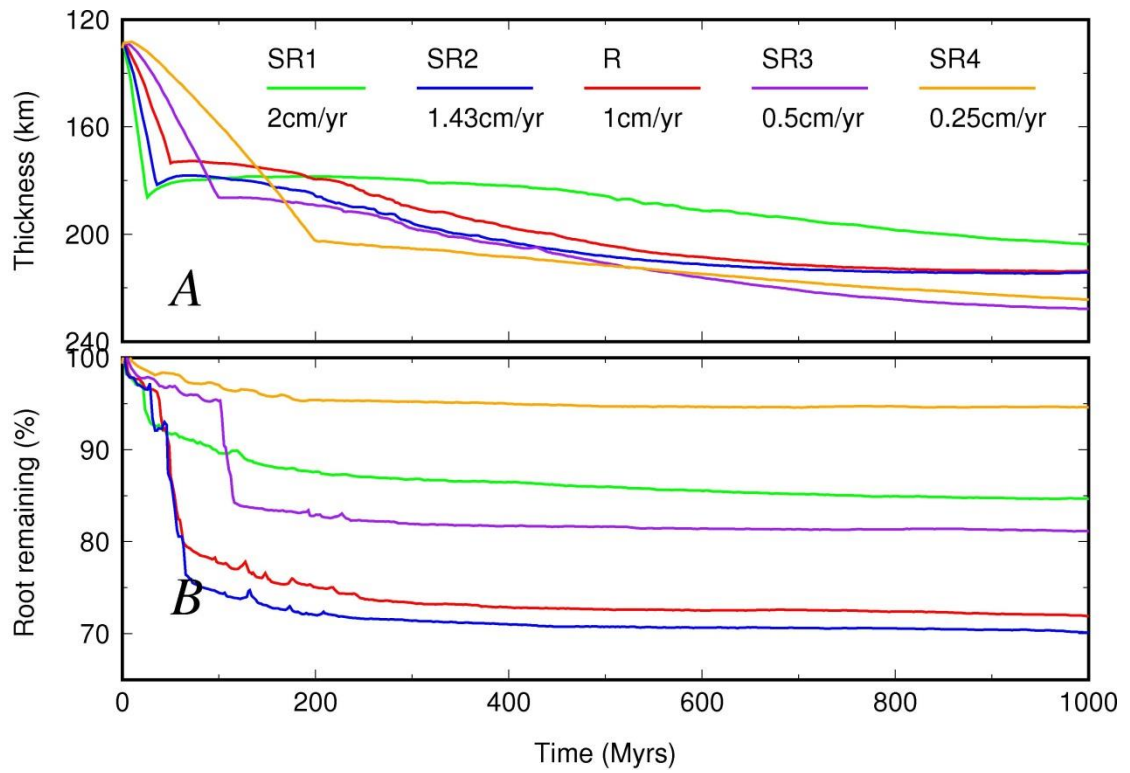
689

690

691

692

Bibliography



693

694 **Fig. 6:** The thickening and recycling of cratonic root material in models with different shortening rates  
695 (Model SR1, SR2, R, SR3, SR4). The same shortening factors ( $\beta=0.62$ ) are applied in these models, which  
696 results in different shortening periods (25Myrs, 35 Myr, 50 Myr, 100 Myr, 200 Myr, respectively).

697

698

699

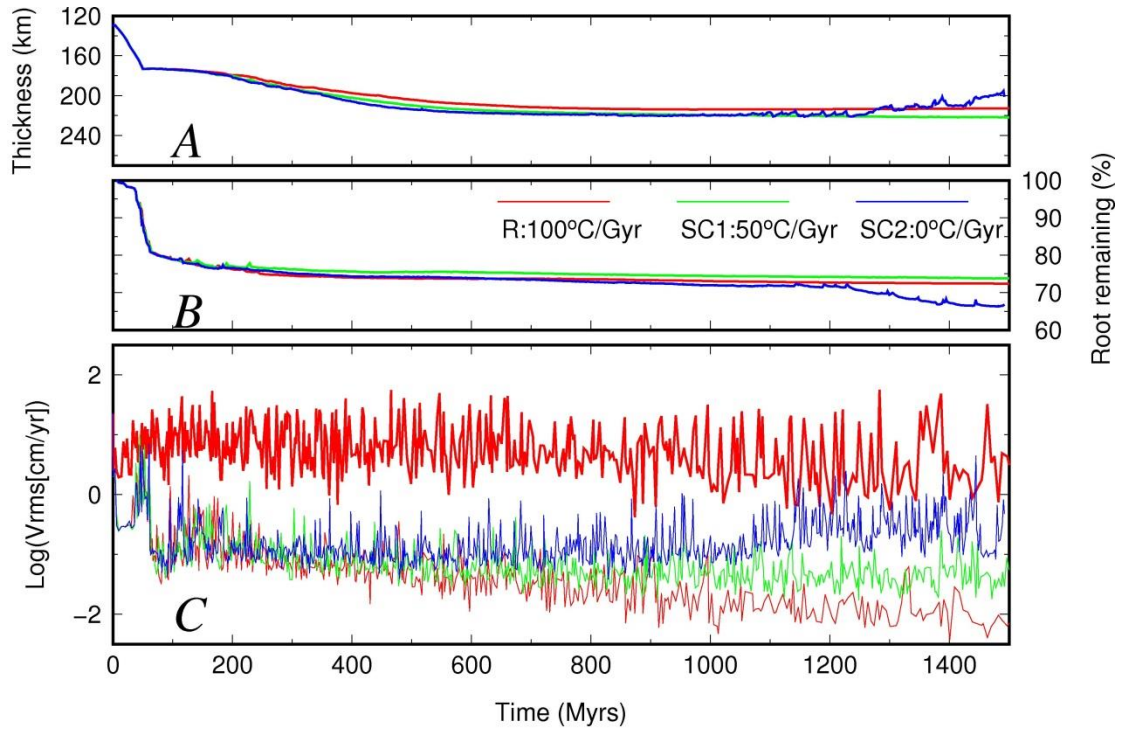
700

701

702



Bibliography



703 **Fig. 7** Thickness (A), remaining root (B) and root-mean-square velocity (C) of the cratonic root material  
704 in models with different secular basal cooling rates. Whereas Model R ( $100^{\circ}\text{C}/\text{Gyr}$ ) and SC1 ( $50^{\circ}\text{C}/\text{Gyr}$ )  
705 remain stable indefinitely, the cratonic root in Model SC2 which has no basal cooling starts to show sig-  
706 nificant thinning and recycling of the root material after  $\sim 1$  Gyr. The thick red line is the average vrms of  
707 the whole model domain in Reference Model R.

708

709

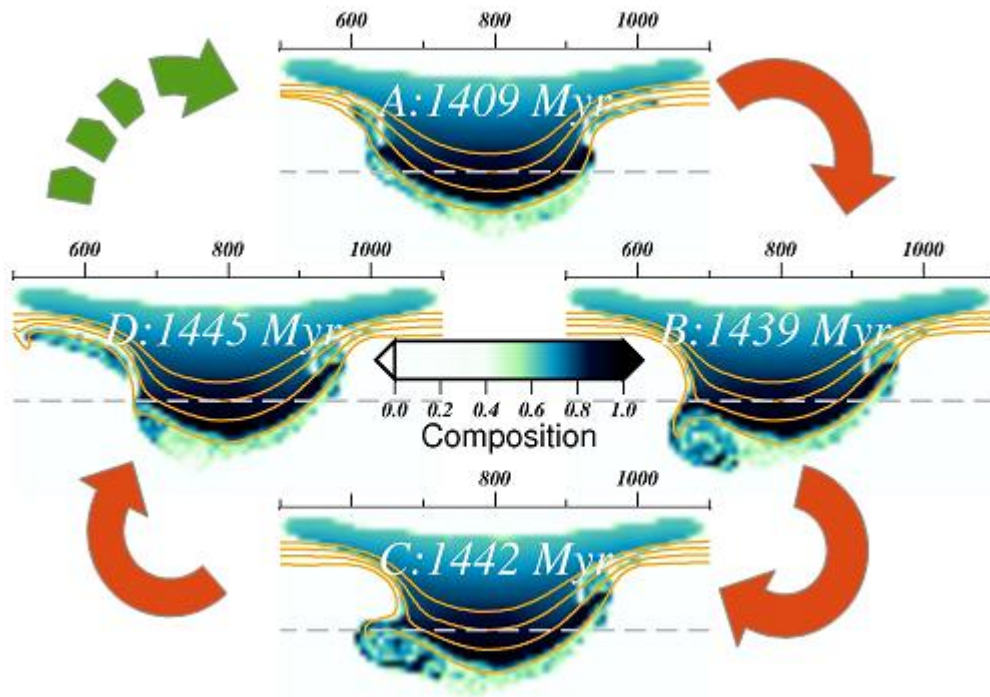
710

711

712

713

714



715

716 **Fig. 8:** Illustration of the oscillatory instability of the cratonic root after 1 Gyr in Model SC2 which has  
 717 no secular cooling of the mantle: the chemical cratonic root undergoes periodic dripping down up-  
 718 welling over several 10s of Myr. The orange curves are isotherms for  $T=1100^{\circ}\text{C}$ ,  $1200^{\circ}\text{C}$ ,  $1300^{\circ}\text{C}$ ,  
 719  $1400^{\circ}\text{C}$ , respectively. The dashed lines mark the depth of 200 km.

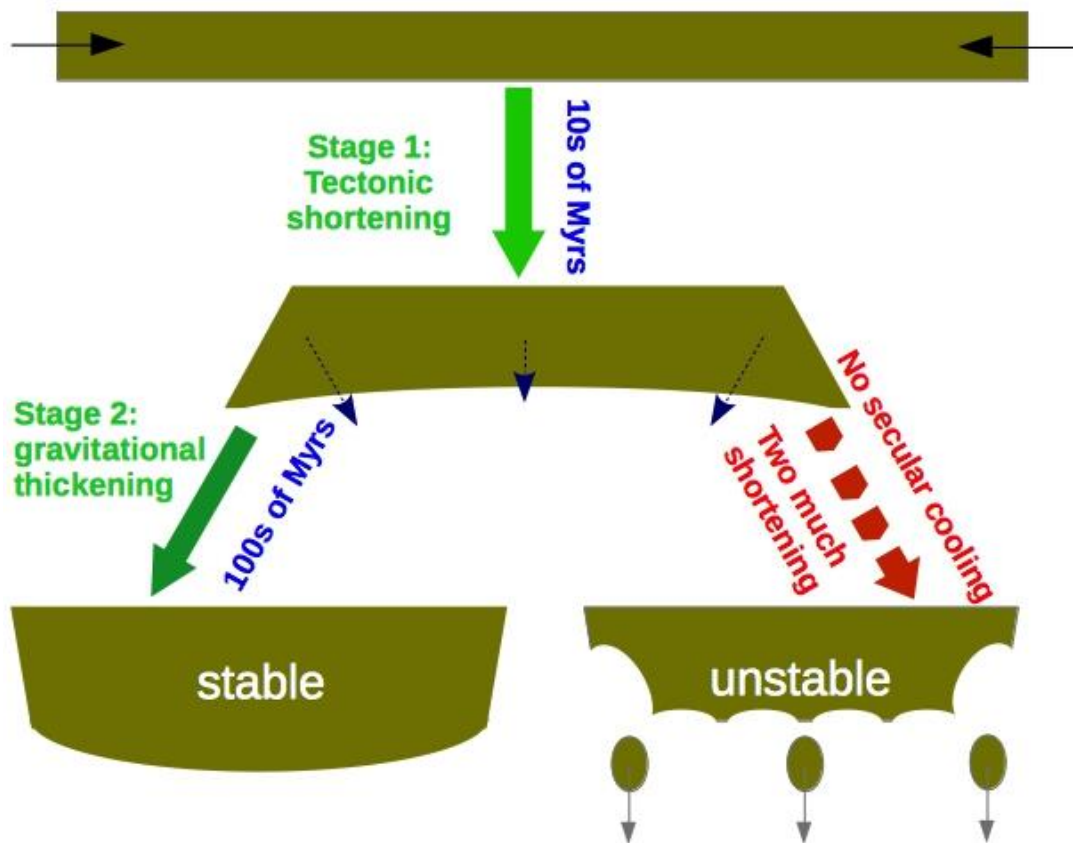
720

721

722

723

724



## Bibliography

725 **Fig. 9:** *The schematic diagram of the two-stage thickening model for the formation of thick cratons re-*  
726 *sulting from numerical simulations. The first stage of thickening is caused by tectonic shortening that last*  
727 *for 10s of Myr, while the second stage is driven by the gravity of the cooling root as a result of thermal*  
728 *equilibrium that lasts for 100s of Myrs. A specific range of Stage 1 shortening (tectonic thickening) is*  
729 *required to introduce Stage 2 (gravitational thickening). Too much tectonic shortening may introduce an*  
730 *unstable root. In addition, mantle secular cooling also has a stabilizing effect on the cratonic root by pre-*  
731 *venting the oscillatory instability observed in Fig. 8.*

732

733

734

735

736